Manipulating Plasma Turbulence in Cross-field Plasma Sources Using Unsteady Electrostatic Forcing

B Rose, A Knoll

Imperial Plasma Propulsion Laboratory, Imperial College, Exhibition Rd, South Kensington, London, SW7 2AZ

E-mail: brbenrose@gmail.com, a.knoll@imperial.ac.uk

Abstract.

Unsteady electrostatic forcing is investigated as a method for manipulating turbulent plasma behaviour within Hall effect thrusters and similar cross-field plasma devices using a simplified 1D-3V azimuthal electrostatic particle-in-cell simulation. A wide range of axial electric field forcing frequencies from 1 MHz up to 10 GHz at amplitudes of $10\,\mathrm{V\,cm^{-1}}$, $50\,\mathrm{V\,cm^{-1}}$ and $100\,\mathrm{V\,cm^{-1}}$ are applied to the plasma and the response is evaluated against a baseline case defined by community benchmark *LANDMARK Test Case 1*. 'Tailoring' of plasma parameters such as the electron cross-field mobility is demonstrated via manipulation of the electron drift instability using unsteady forcing. Excitation of the unstable electron cyclotron modes of the electron drift instability is shown to be able to produce a reduction of the resultant electron cross-field mobility of the plasma by up to 50% compared to the baseline value. Additionally, forcing at the electron cyclotron frequency appears to be capable of increasing cross-field mobility by up to 2000%. Implications of the results for direct drive electric propulsion systems and improved current utilisation efficiencies for Hall effect thrusters are discussed.

Hall effect thruster, electron drift instability, cross-field mobility, plasma turbulence, low temperature plasma: Submitted to: *J. Phys. D: Appl. Phys.*

1. Introduction

The Hall effect thruster (HET), or stationary plasma thruster (SPT), is a form of electric propulsion (EP) system for spacecraft that generates thrust by accelerating the ions of a plasma using crossed electric and magnetic fields [1, 2]. The first Hall thruster flew in 1971 onboard the Soviet METEOR-18 satellite, which used two SPT-60 type thrusters for station keeping maneuvers [3]. Since then, HETs have evolved to become a mainstay of satellite electric propulsion technology. Between 2009 and 2018 over 43% of EP satellites launched into low Earth orbit (LEO) have utilized some form of HET whilst for geostationary Earth orbit (GEO) satellites the percentage is even higher at 57% [3]. Despite their common use, the understanding of the underlying physics defining the systems operation has yet to be fully understood, particularly the ways in which turbulent plasma modes can affect performance [4]. Their design is informed, in many cases, by empirical scaling laws rather than self consistent theory, making optimisation a long, costly and primarily experimental process [5].

A typical HET consists of an annular ceramic channel, terminated by an anode at one end and left open at the opposite end where a hollow cathode external to the channel is located [1, 2]. Ionized propellant is accelerated out of the thruster at high velocity, typically on the order of $10\,\mathrm{km\,s^{-1}}$ [1], by an axial electric field which imparts a small acceleration on the thruster. A strong magnetic field is applied radially creating an E × B region which induces a Hall current on the electrons emitted by the cathode, confining them to the region of high magnetisation and increasing their residence time in the channel [1]. Ions are generated by injecting a neutral propellant, usually Xenon [5], at the anode which is then ionized by the electrons trapped by the E × B drift. The large mass of the ions results in them being less affected by the E × B drift allowing them to freely accelerate out of the channel. HETs are typically described by cylindrical coordinates in three dimensions: the azimuthal dimension around the thruster channel, radial dimension extending outwards radially from the inner magnetic coil and the axial dimension along the direction of the annular channel from anode to cathode end. A diagram showing the key features of the HET is shown in figure 1.

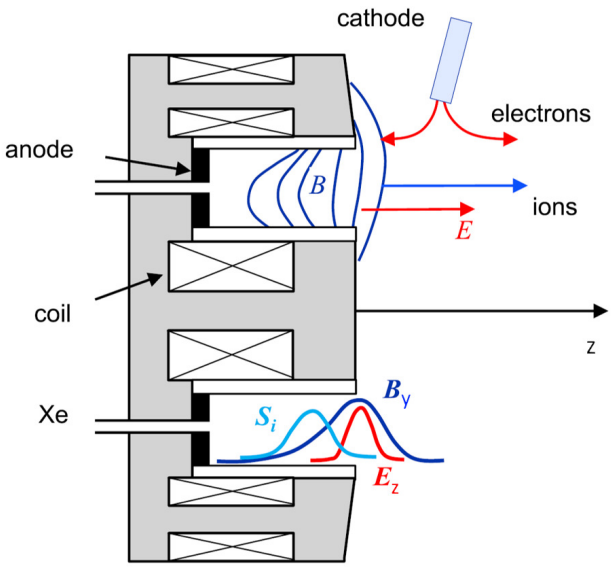

Figure 1: Diagram of HET showing principle of operation, curves E_z and B_y show axial electric field and radial magnetic field strength profiles respectively whilst S_i shows the neutral ionisation rate. Reprinted from J.P. Boeuf and L. Garrigues. E × B electron drift instability in Hall thrusters: Particle-in-cell simulations vs. theory. [6], with permission of AIP Publishing.

Plasma turbulence is a naturally occurring phenomenon that can lead to large discharge current oscillations within HET's and reduce the resultant current utilisation efficiency of the propulsion system. Defining the discharge current supplied to a thruster I_d as the sum of the ion beam current I_b and the electron current I_e, $I_d = I_b + I_e$. The 'useful' current supplied to the thruster is the ion beam current, therefore we can define the current utilisation efficiency as

$$\eta_b = \frac{I_b}{I_d} = \frac{1}{1 + I_e/I_b}. \tag{1}$$

From equation 1 it is evident that an increase in electron current results in a reduction of current utilisation efficiency. One symptom of plasma turbulence within a HET is the so-called 'anomalous' electron cross-field mobility [7] observed when the number of electrons escaping the region of high magnetic field strength within the thruster channel is greater than that predicted by classical theory. This leads to higher

discharge currents as I_e increases and reduced current utilisation efficiency. There are several competing theories for the mechanism by which anomalous mobility occurs such as secondary electron emissions from electron wall collisions [8, 9]; sheath instabilities in radial direction due to secondary electron emission near the thruster channel walls [10, 11]; gradient driven fluid instabilities [12] and instabilities arising as a result of large azimuthal electron drift velocities such as the electron drift instability (EDI) [13, 14]. Whilst the overall anomalous mobility experienced is fundamentally a result of the summation of all these effects, the instability driven mechanism, via the EDI, is suspected to be dominant [15, 16].

Unsteady forcing is a widely explored technique in the field of aerodynamics for controlling non-linear turbulent systems to improve the stall characteristics of airfoils at high angles of attack [17]. A chaotic system, for instance a turbulent boundary layer or, in the case of this investigation, an unstable plasma has a forcing signal applied to it (for example pulsing air jets or, for a plasma, an oscillating electric field) with the goal of tailoring its macroscopic properties. Due to the natural energy pathways between wavemodes in the system, with the correct forcing, energy can be transferred between frequencies and wavenumbers in order to tailor the unsteady dynamics of the system to achieve structured or quasi-periodic behaviour from the chaos [18].

It is the primary aim of this study to demonstrate tailoring of a macroscopic plasma property, the electron cross-field mobility, by manipulation of microscopic plasma instabilities, such as the EDI, in a simplified computational model via the method of unsteady forcing. It is hoped that this analysis will provide a good basis for informing future work into improving the current utilisation efficiencies and performance characteristics of HETs and adjacent cross-field plasma device technologies as a consequence of unwanted plasma dynamics.

2. Method

The theory underlining both the EDI and the electron cross-field mobility is outlined below in a simplified model for unbounded collisionless plasmas along with definitions of useful parameters to the subsequent investigation. The numerical model used to simulate these phenomena is then described along with the experiments performed to investigate the effects of unsteady forcing. The effect of unsteady forcing is quantified by first establishing a baseline case for the plasma where turbulence develops normally. This is then compared to the case with forcing applied and any change in the resultant plasma parameters are identified.

2.1. Electron Drift Instability

Also known as electron-cyclotron drift instability or beam cyclotron instability, the electron drift instability is thought to be a primary factor in driving anomalous transport in Hall effect thrusters [15, 16]. Initially investigated in the context of collisionless longitudinal shocks in space plasmas in the 1960s and 70s [6], the theory behind EDI formation is still an active topic of research. An EDI forms when electron Bernstein modes at high frequencies at multiples of the electron cyclotron frequency Doppler shift towards lower frequencies and the ion acoustic mode frequency range. Once within a similar frequency range, the two modes merge to form the EDI [19].

The dispersion relation, linking wavenumber k and frequency ω, for the EDI has been derived in both three dimensions and one dimension extensively by Ducrocq et al. from the perturbed Vlasov equation [20]. Equation 2 shows the three-dimensional dispersion relationship

$$1 + k^2\lambda_{De}^2 + g\left(\frac{\omega - k_x \mathrm{v}_{\mathbf{E}}}{\Omega_{ce}}, (k_y^2 + k_z^2), k_y^2 r_{ce}^2\right) - \frac{k^2\lambda_{De}^2\omega_{pi}^2}{(\omega - k_z \mathrm{v}_{b,i})^2} = 0 \tag{2}$$

where g is the Gordeev function, $\mathbf{v_E}$ is the electron azimuthal drift velocity and $\mathbf{v}_{b,i}$ is the primary axial ion beam velocity [21]. The wave number vector in three dimensions is $\mathbf{k} = [k_x, k_y, k_z]^T$. λ_{De}, Ω_{ce}, r_{ce} and ω_{pi} denote the Debye length, electron cyclotron frequency, the electron Larmor radius at thermal velocity $\mathrm{v_{the}}$ and the ion plasma frequency respectively.

From Ducrocq et al.'s analysis of equation 2 in the axial-azimuthal plane it has been shown that the stability transitions for the EDI occur when $\omega - k_x \mathrm{v}_{\mathbf{E}} = n\Omega_{ce}$. For the EDI ω is small in comparison to Ω_{ce}, resulting in resonance peaks when $k_x \mathrm{v}_{\mathbf{E}} \approx n\Omega_{ce}$, $n = \pm 1, 2, 3....$ The resultant unstable wavenumbers, the cyclotron harmonics, are denoted nk_0 where $k_0 = \Omega_{ce}/\mathrm{v}_{\mathbf{E}}$ [22]. In the limit where the wavenumber parallel to magnetic field is sufficiently large, such as for a Hall effect thruster with an appropriately sized radial dimension, the relation reduces to a ion acoustic-like dispersion relation with approximate analytical solution [12, 23, 24]

$$\omega_R = \mathbf{k} \cdot \mathbf{v}_{b,i} \pm \frac{k c_s}{\sqrt{1 + k^2\lambda_{De}^2}} \tag{3a}$$

$$\gamma \approx \pm\sqrt{\frac{\pi m_e}{8m_i}}\frac{\mathbf{k}\cdot\mathbf{v_E}}{\left(1+k^2\lambda_{De}^2\right)^{3/2}} \tag{3b}$$

where ω_R and γ are the angular wave frequency and growth rate of the wave respectively, c_s is the ion sound speed and m_i and m_e is the ion and electron mass respectively. Assuming the instability is primarily in the azimuthal dimension, $\mathbf{k} \approx [k_x\, 0\, 0]^T$ and therefore $k \approx k_x$. Setting $\partial\gamma/\partial k = 0$ finds k, ω_R and γ at maximum growth rate

$$[k]_{max} = \frac{\sqrt{2}}{2\lambda_{De}} \tag{4a}$$

$$[\omega_R]_{max} = \mathbf{k}\cdot\mathbf{v}_{b,i} \pm \frac{\sqrt{3}\omega_{pi}}{3} \tag{4b}$$

$$[\gamma]_{max} = \sqrt{\frac{\pi}{27}}\frac{\omega_{pi}\mathrm{v_E}}{\mathrm{v_{the}}}. \tag{4c}$$

The wave phase and group velocities are defined by $\mathrm{v}_\phi = \omega_R/k$ and $\mathrm{v}_g = \partial\omega_R/\partial\mathbf{k}$ respectively. From equation $3a$ we find for the EDI

$$\mathrm{v}_\phi(k) = \hat{\mathbf{k}}\cdot\mathbf{v}_{b,i} \pm \frac{c_s}{\sqrt{1+k^2\lambda_{De}^2}} \tag{5}$$

$$\mathrm{v}_g(k) = \mathbf{v}_{b,i} \pm \hat{\mathbf{k}}\frac{c_s}{\left(1+k^2\lambda_{De}^2\right)^{3/2}} \tag{6}$$

where $\hat{\mathbf{k}} = \mathbf{k}/k$. Evaluating the EDI phase velocity at maximum growthrate we obtain $\mathrm{v}_\phi = \sqrt{3/2}c_s$.

2.2. Electron Cross-field Mobility

The electron cross-field mobility (also known as cross-field transport) describes the electron movement in the axial dimension out of the highly magnetized region of the thruster and is parameterized by $\mu = u_z/E_0$. The cross-field electron mobility is roughly analogous to the axial electron current. Electron cross-field mobility is predicted from the electron momentum conservation equation [25]

$$\begin{aligned} m_\alpha\frac{D\mathbf{u}_\alpha}{Dt} =& q_\alpha\left(\mathbf{E}+\mathbf{u}_\alpha\times\mathbf{B}\right) - \frac{1}{n_\alpha}\nabla p_\alpha \\ & - m_\alpha\sum_\beta \nu_{\alpha\beta}\left(\mathbf{u}_\alpha - \mathbf{u}_\beta\right) \end{aligned} \tag{7}$$

where $D\mathbf{u}_\alpha/Dt$ denotes the total derivative and $\nu_{\alpha\beta}$ the collision frequency of species α with species β. The flow velocity, electric and magnetic field strength, particle charge, density and pressure are denoted by $\mathbf{u}$, $\mathbf{E}$, $\mathbf{B}$, q, n and p respectively. Ignoring the pressure gradient and inertia terms in the axial and azimuthal directions, with a uniform magnetic field in the radial direction, B_0, the momentum conservation equation becomes

$$0 = qn_eE_z - qn_eu_xB_y - m\nu_{en}n_eu_z \tag{8a}$$

$$0 = qn_eE_x - qn_eu_zB_y - m\nu_{en}n_eu_x \tag{8b}$$

Taking into account the presence of gradients and instabilities observed in the azimuthal direction of the thruster [26] and following the analysis of Lafleur [27] we calculate the effective cross-field transport parameter, taking average field quantities from the electron momentum conservation equations giving equation 9 where ν_{en} is the electron-neutral collision frequency.

$$\mu_{\text{effective}} = \frac{\frac{|q|}{m\nu_{en}}}{1+\frac{\Omega_{ce}^2}{\nu_{en}^2}}\left[1 - \frac{\Omega_{ce} < n_eE_x >}{\nu_{en}n_eE_z}\right] \tag{9}$$

For an even more detailed derivation of the cross-field mobility term, taking into account pressure gradient and inertia terms in the axial and azimuthal directions see the work of Lafleur, Baalrud and Chabert [23, 12].

2.3. Description of PIC Simulation

The underlying physics that govern the turbulent behaviour observed within HETs and the effects of unsteady forcing are outlined and modelled using a reduced order one-dimensional three-velocity (1D-3V) azimuthal fully kinetic electrostatic particle-in-cell (PIC) simulation code using Imperial College Plasma Propulsion Laboratory's (IPPL) *PlasmaSim* written in *Julia* [28]. Previous authors have concluded an azimuthal 1D-3V model is sufficient for capturing the plasma dynamics responsible for both the EDI development and resultant anomalous electron mobility that is under investigation [29]. A simplified model of the HET reduces the complexity of the interactions between the many different plasma modes that exist in a real thruster, making analysing the links between the two properties under investigation far more tractable along with having a significantly reduced computational cost.

PIC simulation is a kinetic method for plasma simulation, representing electrons and ions as groups of 'super-particles' moving according to the particle equations of motion on a grid of cells used for calculating the statistical thermodynamic and electromagnetic properties within a plasma [30]. *PlasmaSim* has been validated for use in three 1D-3V cases for the axial, radial and azimuthal directions of a HET respectively against other plasma models and experimental data [31], the branch used in this investigation is derived from the azimuthal 1D-3V electrostatic method popularized by Birdsall and Langdon [30] using the hard sphere model of Bird to model particle collisions [32]. Unless otherwise stated it should be assumed that the PIC model is identical to that outlined by Birdsall and Langdon. The directions x, y and z denote the azimuthal, radial and axial directions of the Hall effect thruster respec-

tively as shown in figure 2.

Given the technical complexity of producing a functioning PIC code it is necessary to rigorously validate the results of any new code with respect to available test cases and benchmarks provided by the community [7]. Furthermore, in order to identify the effects of applying unsteady forcing to the plasma, a suitable baseline simulation configuration to compare to had to be established. *LANDMARK Test Case 1* [29] was identified as a suitable baseline for both validation and comparison purposes.

Figure 2a shows a diagram of the physical locations of the simulated dimension (dashed line), along which Poisson's equation is satisfied, and particle tracking domain (highlighted surface) in *PlasmaSim* on a reference SPT-100 thruster, reproduced with permission from Tejeda et al. [33]. Figure 2b shows the two dimensionalized version of the simulated dimension and particle tracking domain 'unwrapped' from the annular channel along with particle boundary conditions.

To accurately reproduce the baseline test case the following boundary conditions were implemented for the particles and electric field. Initially electrons, neutrals and ions are all generated with a randomized Maxwellian thermalized velocity at a given temperature, T_{e0}, T_{n0} and T_{i0} respectively, and randomized position within the particle tracking region. Sizes of the superparticles are set according to specified number densities, n_0 for electrons and ions and n_{n0} for neutrals. The azimuthal boundary condition is periodic, with Poisson's equation solved numerically using the finite difference method with Dirchelet boundary conditions of $\phi_{x=0} = \phi_{x=X_{max}} = 0$ where particles passing outside the limits of $x > X_{max}$ or $x < 0$ are re-introduced at the same velocity on the other side of the domain. In order to simplify the modelling of the radial dimension of the HET, another periodic boundary condition was used which again reintroduced particles which left the extents of the simulation domain, $y > Y_{max}$ or $y < 0$, on the other side of the domain. In the axial dimension, electrons passing out of the domain at the anode end ($z = 0$) were eliminated before being reintroduced at a random azimuthal location at the cathode end ($z = Z_{max}$) with a thermalized velocity of temperature T_{e0}. The axial component of the velocity vector is enforced to be into the particle tracking domain to prevent hot electrons being eliminated straight after reinitialisation. Similarly for the ions, upon reaching the cathode end they are eliminated and reintroduced in a similar fashion at the anode end with temperature T_{i0}. Neutral particles are specularly reflected at the axial particle tracking boundary. The static electric and magnetic field strengths, E_0 and B_0 are set in the axial and radial directions respectively.

Collisions between charged particles and neutrals were modelled using the Direct Simulation Monte Carlo (DSMC) method with expected particle collision frequencies between species α and β obtained using the hard sphere model of Bird where the collision frequency $\nu_{\alpha\beta} = n_\alpha \overline{\sigma_{\alpha\beta} \mathrm{v}}$ and the collision cross-section $\sigma_{\alpha\beta} = \pi(r_\alpha + r_\beta)^2$ where r is the Van-der Walls radius of the colliding particle [32].

Given the statistical nature of PIC simulation *Julia's* [28] inbuilt random number generator using the *Xoshiro256++* algorithm is used to generate independent trial runs of each scenario using a different random number generator seed before averaging to remove the effects of statistical noise. Limitations on the simulation parameters for the spatial discretisation of the modelled dimension (Δx) are given by the requirement that Δx must be less than λ_{De} to resolve the Debye length of the plasma and not simply capture collective effects. The time step of the simulation is required to resolve both the electron plasma (Δt_{pe}) and cyclotron frequency (Δt_{ce}) from Nyquists criterion, and satisfy the Courant-Freidrichs-Lewey condition (Δt_{CFL}) which are given by below [30]

$$\Delta t_{pe} < 2\pi/\omega_{pe} \tag{10a}$$

$$\Delta t_{ce} < 2\pi/\Omega_{ce} \tag{10b}$$

$$\Delta t_{CFL} < \Delta x/|\mathrm{v}_{th_e}| \tag{10c}$$

$$\Delta x < \lambda_{de}. \tag{10d}$$

An additional safety factor of 25 is then applied to the minimum time step.

The electron cross-field mobility parameter can be calculated numerically from the simulation particles by evaluating the average axial velocity of of the electrons according to equation 11 where N is the number of electron super-particles at each time step.

$$\mu_{\mathrm{PIC}} = \frac{\sum_{j=1}^{N} \mathrm{v}_{jz}}{N E_0}. \tag{11}$$

2.4. PIC Simulation Baseline Definition

The key publications laying out the conditions and expected results of the baseline configuration are given in *Nonlinear structures and anomalous transport in partially magnetized E × B plasmas* by Janhunen et al. [22] and *Theory for the anomalous electron transport in Hall effect thrusters I & II* by Lafleur et al. [27, 24] which were used in the validation of the results obtained by *PlasmaSim*. The baseline plasma properties used for the initialisation of the simulation are given in

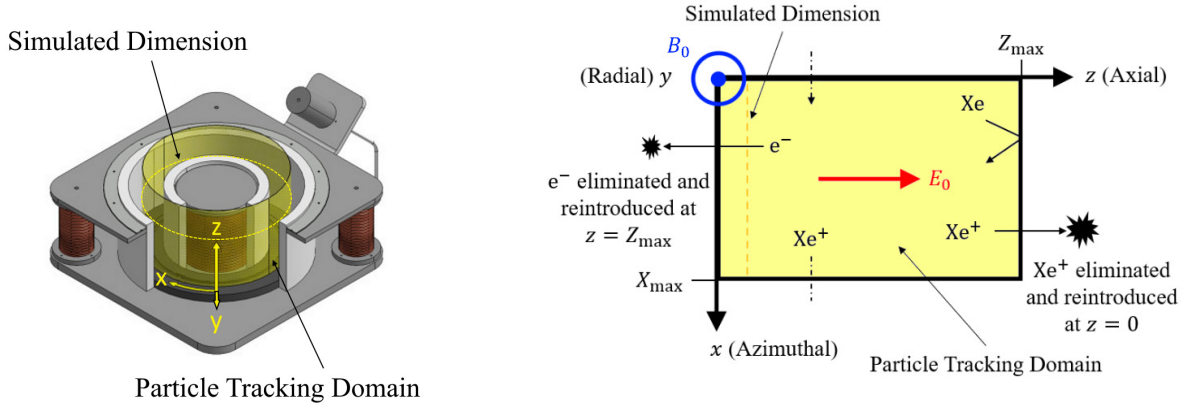

(a) Simulated dimension and particle tracking domain

(b) 2D simulation domain showing boundary conditions

Figure 2: *PlasmaSim* simulation domain

table 1.

Table 1: Baseline operating and numerical parameters used in the PIC simulations

Plasma Property	Value
T_{e0} [eV]	2.0
T_{i0} [eV]	0.1
T_{n0} [K]	300
B_0 [T]	0.02
E_0 [V cm^{-1}]	200
n_{n0} [m^{-3}]	1.0×10^{18}
n_0 [m^{-3}]	1.0×10^{17}

Simulation parameters such as the time step, data capture frequency and spatial discretisation were tuned to satisfy the conditions given by equations 10*a*-10*d* to reduce numerical inaccuracy in the model and achieve an accurate depiction of the EDI and cross-field mobility development. The final simulation parameters settled on are shown in table 2. Where possible, both the baseline plasma properties and the simulation parameters were chosen to closely resemble the key publications outlining the benchmark. Results from a mesh refinement study confirmed that a sufficient number of cells (NG) for resolving the instability was 175 in the x dimension with a time step (t_{step}) of 1×10^{-11} s. A data capture rate (t_{write}) of 1×10^{-10} s was selected by Nyquist's criterion to capture interesting plasma behaviour at frequencies up to and including the electron plasma frequency whilst reducing the the size of the simulation output files. The extents of the simulation domain X_{max}, Y_{max} and Z_{max} were chosen as 0.005 m, 0.0075 m and 0.01 m respectively. 100 super particles per cell for each species (N/NG) was selected from literature as an appropriate number for initialisation of the simulation. Promisingly, the simulation parameters were within the bounds of those proposed previously by Lafleur et al. [27] for the same test case.

Table 2: Simulation parameters

Simulation Parameter	Value
t_{step} [s]	1.0×10^{-11}
t_{write} [s]	1.0×10^{-10}
NG	175
N/NG	100
X_{max} [m]	0.005
Y_{max} [m]	0.0075
Z_{max} [m]	0.01

2.5. Application of Unsteady Forcing

The primary method to affect unsteady forcing was by varying the axial electric field which was thought could provide a mechanism for manipulating azimuthal instabilities and hence the cross-field mobility of the plasma. It had previously been observed that forcing the axial electric field could lead to changes in the temporal spectral energy distribution of the azimuthal electric field however specific effects of forcing over a wide band of forcing frequencies had yet to be fully characterized.

In a real HET, axial electric field forcing could be accomplished by varying the potential of the anode or the cathode to achieve the desired electric field. This has previously been suggested by Tejeda et al. [33] but not yet tested experimentally. The axial electric field in a HET is non-uniform as shown in figure 1, but, given the 1D-3V azimuthal version of *PlasmaSim* does not resolve Poisson's equation in this direction, the ax-

ial electric field profile is instead simplified to a uniform field varying in time with field strength given by $E_z = E_0 + A_{\mathrm{EF}} \sin \omega_{\mathrm{EF}} t$, where E_0 is the average static electric field strength and $A_{\mathrm{EF}} \sin \omega_{\mathrm{EF}} t$ is the superimposed oscillation. A_{EF} is the amplitude and ω_{EF} is the frequency of the forcing of the electric field, t is the simulation time.

3. Results

3.1. Simulation Validation

The plasma distributions obtained in *PlasmaSim* for the parameters specified for the baseline test case are shown in figure 3. Both the electron density and the azimuthal electric field show wave-like behaviour with high wavenumber oscillations over the first 500 ns giving way to low wavenumber, progressively more chaotic, high amplitude oscillations as the instability saturates towards 4000 ns.

The wavenumber and frequency of the wave like behaviour can be calculated from the electric field distribution by counting peaks along lines XX and YY of figure 4 respectively after saturation. The wave phase speed can be evaluated from $\Delta x/\Delta t$. This method gives a wave phase speed of $5.4 \times 10^3\,\mathrm{m\,s^{-1}}$, wave number of $4.4 \times 10^3\,\mathrm{rad\,m^{-1}}$ and a frequency of $2.7 \times 10^7\,\mathrm{rad\,s^{-1}}$. Given the averaged electron temperature after 4 µs rises to approximately $15 \times T_{e0}$ the Debye length of the plasma would have increased to 1.3×10^{-4} m. Using equations 4*a* and 6 we calculate an expected wavenumber at maximum growthrate $[k]_{max}$ of $5.5 \times 10^3\,\mathrm{rad\,m^{-1}}$, frequency $[\omega_R]_{max}$ of $2.1 \times 10^7\,\mathrm{rad\,s^{-1}}$ and phase velocity $\mathrm{v}_\phi([k]_{max})$ of $4.7 \times 10^3\,\mathrm{m\,s^{-1}}$ for the EDI. The results show a good agreement with those obtained from the analytical dispersion relationship for the wavenumber of maximum growthrate. Phase velocity, wavenumber and frequency show a 15%, 20% and 29% error from the theoretical values respectively which was deemed within acceptable bounds suggesting *PlasmaSim* is accurately modelling the expected physics of the EDI. k, ω and v_ϕ of the resultant wave behaviour appears to be closely related to the wavenumber of maximum growthrate $[k]_{max}$.

The dispersion relationship of the EDI was calculated numerically taking a two-dimensional fast Fourier transform (2DFFT) of the azimuthal electric field field from *PlasmaSim* in *MATLAB* [34] to convert it to a wavenumber-frequency diagram shown in figure 5. The numerical and analytical dispersion relationships show good agreement, with the wavenumber of largest growthrate in figure 5 being close to the analytically calculated value of $[k]_{max}$ and $[\omega_R]_{max}$ for the EDI

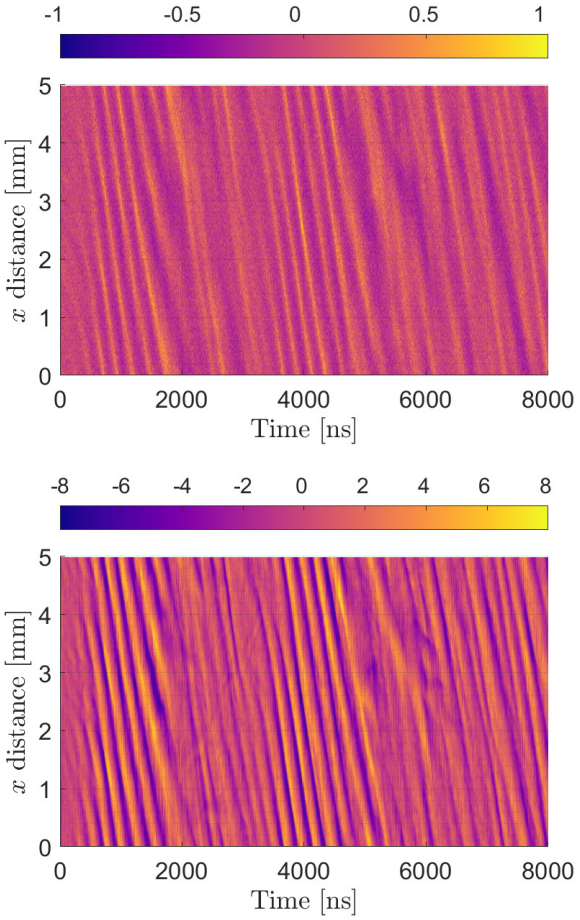

Figure 3: (a) Normalized electron number density $(n_e(x,t) - n_0)/n_0$ and (b) azimuthal electric field strength E_x/E_0 for baseline test case parameters

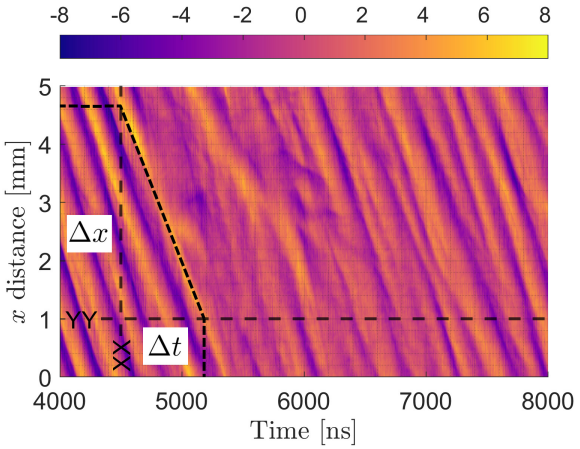

Figure 4: Normalized azimuthal electric field strength E_x/E_0 distribution annotated to calculate wavenumber, frequency and wave speed of resultant wave-like behaviour

from equation 4*a* and 4*b*. These results were compared to Lafleur et al.'s [12] results finding the same dispersion relationship despite Lafleur et al. using a 2D-3V axial-azimuthal PIC model. This gives confidence in the one dimensional model retaining enough complexity to model the EDI sufficiently despite the dimensionality reduction.

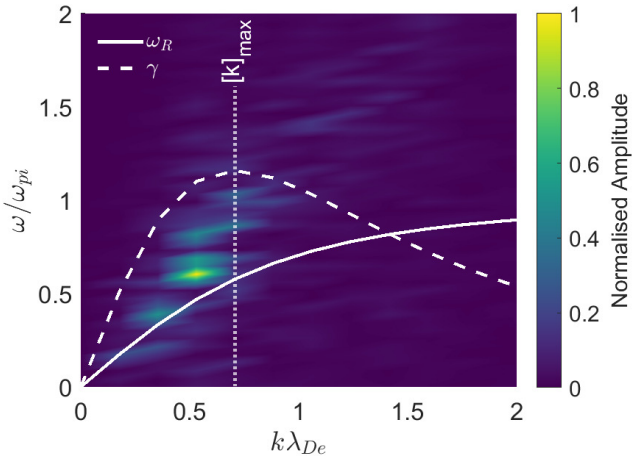

Figure 5: Wavenumber-frequency diagram for wave-like behaviour exhibited by azimuthal electric field showing contour of numerically obtained dispersion relationship and a dashed line showing the predicted analytical dispersion relationship from equation 3*a* (growth rate γ scaled by a factor of 12)

The electron cross-field mobility calculated from equation 11 and averaged over the time period after instability saturation (6 µs - 10 µs) was found as $5.38\,\mathrm{m^2\,V^{-1}\,s^{-1}}$. To reduce the effects of statistical variation the result was averaged over 5 independent simulation runs with a standard deviation of $0.94\,\mathrm{m^2\,V^{-1}\,s^{-1}}$, agreeing with the cross-field mobility parameter obtained by Lafleur [27] for similar simulation parameters.

3.2. Effect of Unsteady Forcing

Initial investigation focused on applying forcing at frequencies at or near to the fundamental plasma frequencies, the electron cyclotron frequency Ω_{ce}, the electron plasma frequency ω_{pe} and the ion plasma frequency ω_{pi}. Three forcing amplitudes of $10\,\mathrm{V\,cm^{-1}}$, $50\,\mathrm{V\,cm^{-1}}$ and $100\,\mathrm{V\,cm^{-1}}$ were tested. The resulting cross-field mobility increased significantly from the baseline value by a factor of over twenty times when the forcing frequency was set to the electron cyclotron frequency whilst only a small increase was noted when forcing at the electron plasma frequency as shown in figure 6. A slight reduction in cross-field mobility was observed forcing at the ion plasma frequency, however this was only statistically significant at the forcing amplitude of $50\,\mathrm{V\,cm^{-1}}$.

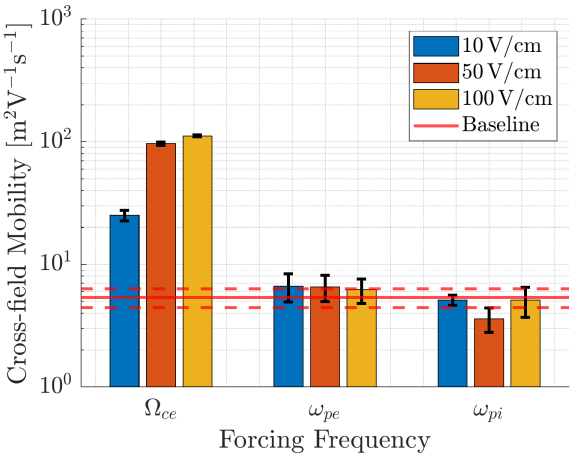

Figure 6: Electron cross-field mobility of plasma for ω_{EF} of specified plasma fundamental frequency at specified forcing amplitudes A_{EF} where error bars and dashed red line show one standard deviation from the value

The temporal spectral amplitude distribution for the azimuthal electric field was compared with the baseline distribution for each forcing frequency. To reduce the effects of statistical noise the amplitude spectrum for the baseline test case was averaged over 5 independent simulation runs to obtain the expected distribution whilst the amplitude spectrum for the forced case was averaged over 3 independent runs. Significant divergences from the baseline distribution were identified for forcing frequencies matching the electron cyclotron frequency and the ion plasma frequency as can be seen from figures 7 and 8 respectively. Forcing at the electron cyclotron frequency resulted in a reduction in spectral amplitude around the frequency of maximum growthrate of the EDI $[\omega_R]_{max}$ whilst all other frequencies saw an increase in amplitude, particularly for frequencies exceeding the Hall circulation frequency ω_E. Conversely, forcing at the ion plasma frequency lead to a increase in spectral amplitude for frequencies between ω_{pi} and ω_E with a reduction in spectral amplitude for frequencies greater than ω_E or lower than ω_{pi}, the amplitude of the peaks associated with the electron cyclotron frequency and its resonances appeared to be damped when forcing at this frequency was applied.

To attempt to fully characterize the effects of unsteady forcing a wider range of frequencies from the MHz range up to the GHz range were investigated. Simulations were run with forcing frequencies ω_{EF}

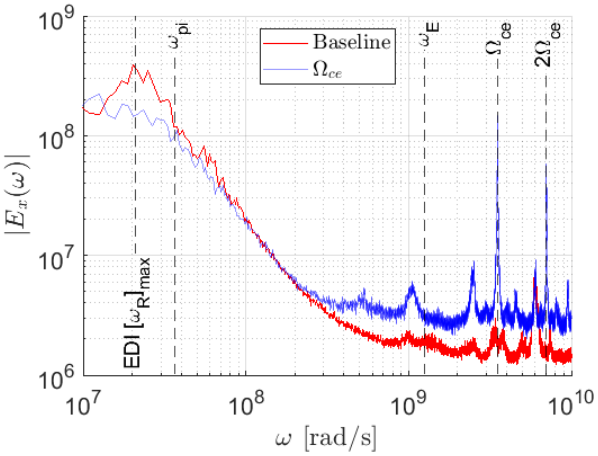

Figure 7: Azimuthal electric field spectral amplitude distribution of baseline case compared to case forced at electron cyclotron frequency with A_{EF} of $100\,\mathrm{V\,cm^{-1}}$

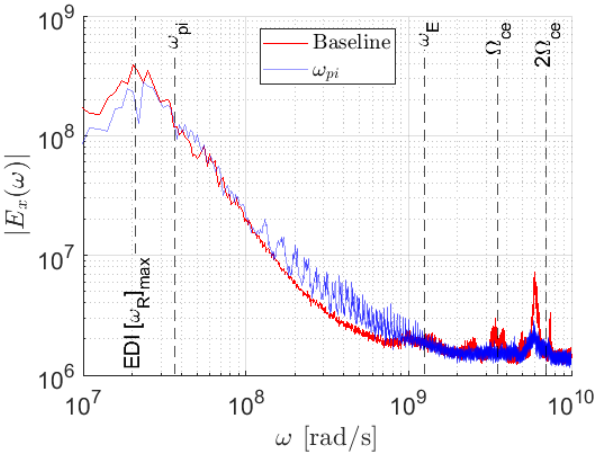

Figure 8: Azimuthal electric field spectral amplitude distribution of baseline case compared to case forced at ion plasma frequency with A_{EF} of $100\,\mathrm{V\,cm^{-1}}$

from 1×10^6 Hz to 1×10^{10} Hz in logarithmic steps, i.e 10^6 Hz, $10^{6.1}$ Hz, $10^{6.2}$ Hz etc, to encompass the whole range. Again, three forcing amplitudes A_{EF} of $10\,\mathrm{V\,cm^{-1}}$, $50\,\mathrm{V\,cm^{-1}}$ and $100\,\mathrm{V\,cm^{-1}}$ were tested to quantify the effects of varying forcing amplitude. The resultant power spectrum data and associated cross-field mobility was averaged over 3 independent simulation runs similarly to above.

Approximate forcing effects can be grouped roughly according to the qualitatively observed effects on different frequency bands. To aid discussion, the 'low' frequency band shall be frequencies below the ion plasma frequency ω_{pi}, 'mid-range' frequencies shall be between ω_{pi} and the Hall circulation frequency ω_E and 'high' frequencies shall be frequencies above the Hall circulation frequency. Forcing frequencies ω_{EF} in the low frequency range, below the ion plasma frequency, typically resulted in spectral amplitude reduction in the low frequency range as demonstrated in figure 9 however the amplitude around the EDI maximum growthrate frequency $[\omega_R]_{\max}$ remained approximately the same. Furthermore above ω_{pi} the spectral amplitude showed a characteristic reduction, particularly around the electron cyclotron frequency resonances and the Hall circulation frequency. No obviously resonant behaviour was observed at multiples of the forcing frequency in this range.

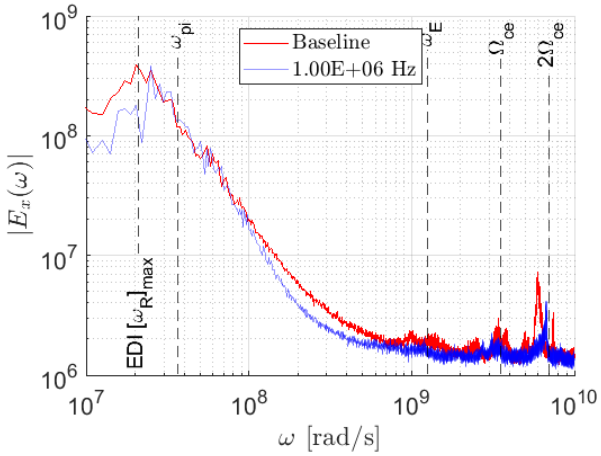

Figure 9: Azimuthal electric field spectral amplitude distribution of baseline case compared to typical case forced in low frequency range (1.00×10^6 Hz) with A_{EF} of $50\,\mathrm{V\,cm^{-1}}$

Mid-range forcing for ω_{EF} between the ion plasma frequency ω_{pi} and the Hall circulation frequency ω_E, an example of which is demonstrated in figure 10, resulted in interesting behaviour whereby large peaks in amplitude centered on the forcing frequency ω_{EF} and its resonances appear in the spectral amplitude distribution for the azimuthal electric field, demonstrating a coupling between the axial and azimuthal electric field behaviour. Mid-range forcing also appears to reduce the spectral amplitude in both the high and low frequency ranges. As the forcing frequency approaches ω_E the amplitude of the electron cyclotron peak and its resonances becomes increasingly damped, potentially indicating a coupling between mid-range frequency modes and the high frequency electron cyclotron modes.

Figure 11 shows a characteristic response of the plasma when forced within the high frequency range, demonstrating the observed phenomena of 'frequency lock-in' [18]. When the plasma is forced at a frequency

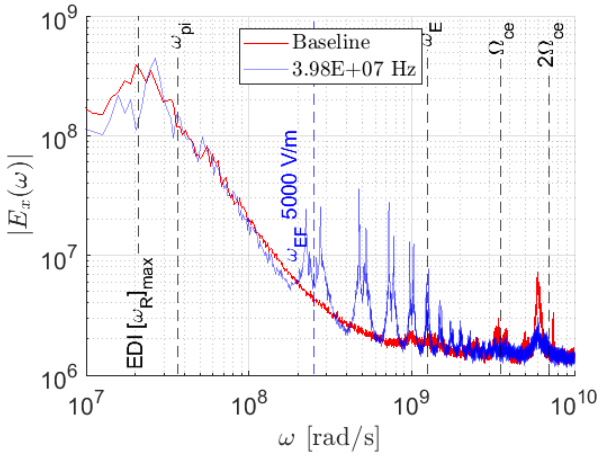

Figure 10: Azimuthal electric field spectral amplitude distribution of baseline case compared to typical case forced in frequency mid-range (3.98×10^7 Hz) with A_{EF} of $50\,\mathrm{V\,cm^{-1}}$

close to the electron cyclotron frequency the peak typically located at Ω_{ce} is observed to shift slightly away from its usual position towards the forcing frequency or lock-in frequency. Similar behaviour is observed at the resonances of the electron cyclotron frequency, sometimes with a significant amplitude reduction or peak sharpening at the other resonances. When ω_{EF} is not located near an electron cyclotron frequency resonance, no significant change in the spectral amplitude distribution is observed. Forcing close to the Hall circulation frequency ω_{E} and its resonances appears to amplify the other Hall circulation resonances.

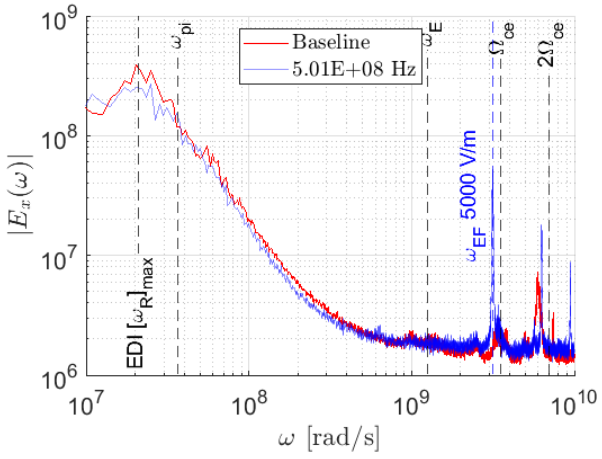

Figure 11: Azimuthal electric field spectral amplitude distribution of baseline case compared to typical case forced in high frequency range (5.01×10^8 Hz) with A_{EF} of $50\,\mathrm{V\,cm^{-1}}$

Generally speaking, increasing the amplitude of the forcing function appears to increase the change in spectral amplitude observed. Forcing at $10\,\mathrm{V\,cm^{-1}}$ does not appear to significantly reduce the low frequency spectral amplitude compared to forcing at $50\,\mathrm{V\,cm^{-1}}$ when ω_{EF} is in the low frequency range. When ω_{EF} is in the mid-range to high frequency region the response for $10\,\mathrm{V\,cm^{-1}}$ amplitude is similar to that observed for the higher forcing amplitudes tested.

The cross-field mobility calculated for the plasma at each forcing condition over a range of frequencies is shown in figure 12, 13 and 14 for forcing amplitudes of $10\,\mathrm{V\,cm^{-1}}$, $50\,\mathrm{V\,cm^{-1}}$ and $100\,\mathrm{V\,cm^{-1}}$ respectively and compared to the expected value calculated from the unforced baseline case. To take into account the statistical variation in the results output by the PIC algorithm the figures show both the mean value and the region of one standard deviation from the mean. The mean baseline cross-field mobility is represented by a horizontal red line with the standard deviation of this shown by two dashed horizontal red lines. Statistically significant results which showed a deviation of the cross-field mobility from the baseline value were identified using a two sample, two tailed t test at the 5% confidence level and are circled in red.

As expected from the prior investigation of plasma fundamental frequencies, for all three forcing amplitudes tested the cross-field mobility peaks when the forcing frequency is close to Ω_{ce} with cross-field mobility increasing with amplitude. There is a reduction in cross-field mobility by a factor of up to a half relative to the baseline test case for forcing frequencies close to the frequency of the fundamental cyclotron harmonic $\omega_R(k_0)$ and its resonances, this is most pronounced for a forcing amplitude of $50\,\mathrm{V\,cm^{-1}}$. At the same forcing amplitude, the cross-field mobility appears to be reduced somewhat for forcing frequencies in the range between the ion plasma frequency and the Hall circulation frequency, no such effect is distinguishable for the other trial forcing amplitudes. Forcing at $10\,\mathrm{V\,cm^{-1}}$ appears to result in the smallest deviation in cross-field mobility to the baseline case.

4. Discussion

4.1. Significance of frequency of cyclotron harmonics

The reduction in cross-field mobility in the low frequency range is centered upon the frequency of the EDI's unstable cyclotron harmonics $\omega_R(k_0)$, $\omega_R(2k_0)$, $\omega_R(3k_0)$, $\ldots$, $\omega_R(nk_0)$. The frequencies of these harmonics are calculated from the dispersion relationship for the EDI from the equation of angular wave frequency $3a$. Substituting in the unstable

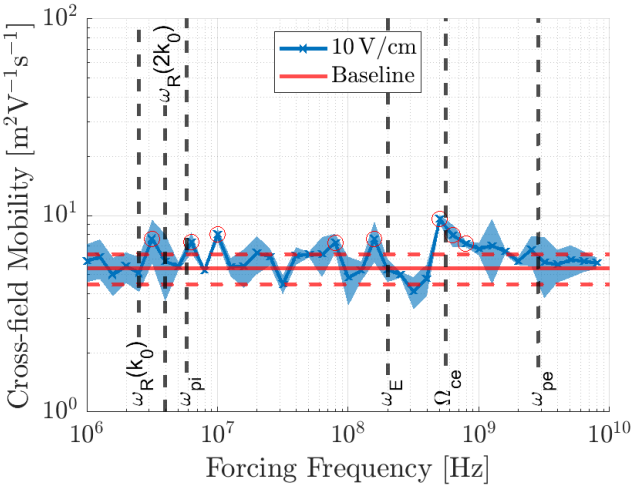

Figure 12: Cross-field mobility of plasma excited at given forcing frequency ω_{EF} at forcing amplitude A_{EF} of $10\,\mathrm{V\,cm^{-1}}$

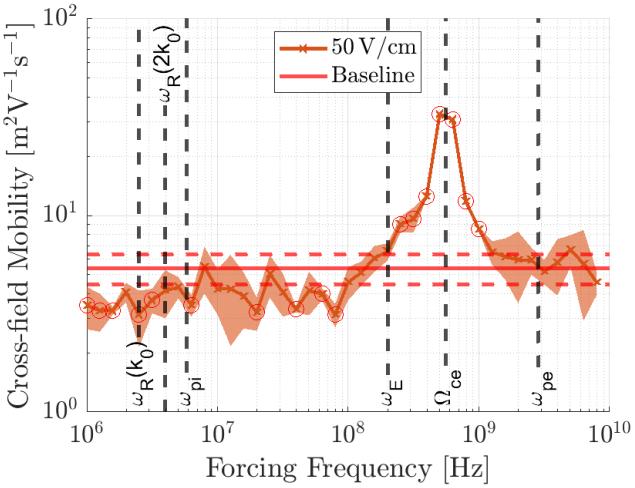

Figure 13: Cross-field mobility of plasma excited at given forcing frequency ω_{EF} at forcing amplitude A_{EF} of $50\,\mathrm{V\,cm^{-1}}$

cyclotron wavenumbers nk_0 to this equation gives the wave frequency as

$$\omega_R(nk_0) = \pm\frac{nk_0c_s}{\sqrt{1+(nk_0)^2\lambda_{De}}} \tag{12}$$

where $n = 1, 2, 3\ldots$ and λ_{De} is a function of the electron temperature. Forcing at the frequency $\omega_R(nk_0)$ was observed to reduce the temporal spectral amplitude of frequencies other than those corresponding to an unstable wavemode in the low frequency region, potentially as a result of energy pathways amplifying the unstable EDI mode or as a result of frequency lock-in type behaviours. Figure 15 demonstrates this behaviour for forcing at the frequency of the fundemental cyclotron harmonic $\omega_R(k_0)$ for the temporal spectral distribution. Observing the region of the spectrum between $1\times10^7\,\mathrm{rad\,s^{-1}}$ and $1\times10^8\,\mathrm{rad\,s^{-1}}$, the spectral amplitude for the forced plasma shows peaks at $\omega_R(k_0)$, $\omega_R(2k_0)$ and $\omega_R(3k_0)$ with a reduction in spectral amplitude everywhere else compared to the baseline case. Similar results were observed for cases where forcing is applied at the frequency of two other unstable cyclotron harmonics $2k_0$ and $3k_0$.

Figure 14: Cross-field mobility of plasma excited at given forcing frequency ω_{EF} at forcing amplitude A_{EF} of $100\,\mathrm{V\,cm^{-1}}$

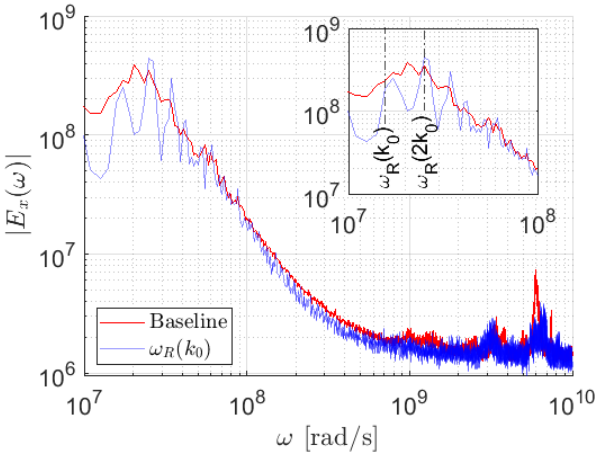

Figure 15: Azimuthal electric field temporal spectral amplitude distribution of baseline case compared to case forced at fundamental cyclotron frequency k_0 with A_{EF} of $50\,\mathrm{V\,cm^{-1}}$

Comparing the development of the spatial spectral amplitude distribution for the azimuthal potential field of the baseline case shown in figure 16 with that forced at the frequency of the fundamental cyclotron

harmonic $\omega_R(k_0)$ shown in figure 17 it can be seen that forcing induces a reduction in spectral amplitude for wavemodes which are not excited, $2k_0$, $3k_0$,..., whilst the excited wavemode k_0 sees an increase in amplitude. Counterintuitively we see a reduction not an increase in cross-field mobility by forcing at the frequency of the unstable modes of the EDI. Referring back to equation 9, it is known that the cross-field mobility is dependant on the cross-correlation term $< n_e E_x >$ which increases for larger electric field oscillation amplitudes as discussed previously. One possible theory for the larger cross-field mobility of the baseline case is because multiple unstable cyclotron harmonic modes are excited, resulting in chaotic behaviour where the superposition of two or more cyclotron harmonic modes can result in large amplitude fluctuations. For the forced case, forcing at the fundamental cyclotron harmonic $\omega_R(k_0)$ results in excitation of only one of the unstable cyclotron harmonics and attenuation of the others after the plasma locks-in on the frequency. Given only one wavemode is excited there is less opportunity for superposition which would lead to large amplitude oscillations in the azimuthal electric field that would cause the increase in cross-field mobility. Another possible theory for the reduction could be due to the forcing causing E_x and n_e to oscillate out of phase, reducing $< n_e E_x >$.

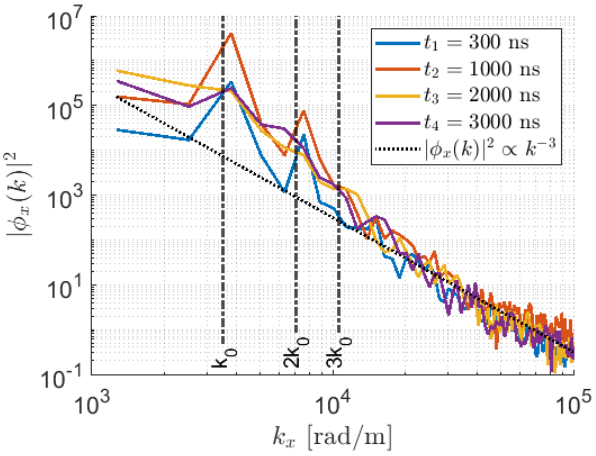

Figure 16: Development of plasma azimuthal potential field spatial spectral amplitude distribution of baseline case over first4 µs of simulation time with A_{EF} of $50\,\mathrm{V\,cm^{-1}}$

4.2. Significance of the electron cyclotron frequency

Forcing close to the electron cyclotron frequency led to a large increase in cross-field mobility. It is theorised that this could be a result of disruption to the circular

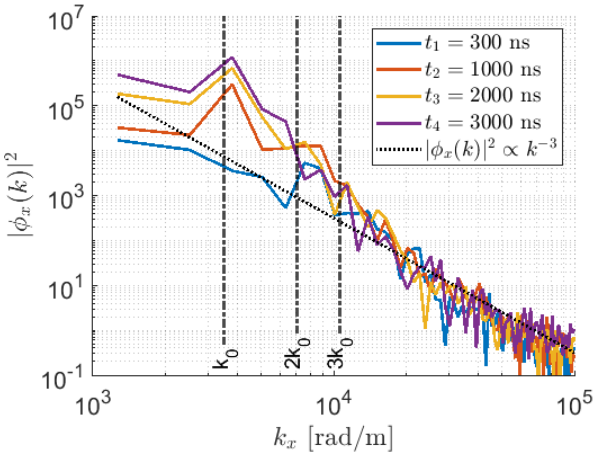

Figure 17: Development of azimuthal potential field spatial spectral amplitude distribution of plasma forced at fundamental cyclotron frequency $\omega_R(k_0)$ over first4 µs of simulation time with A_{EF} of $50\,\mathrm{V\,cm^{-1}}$

motion of the electrons normally oscillating at that frequency in the $\mathbf{E} \times \mathbf{B}$ field, causing the electrons to break confinement. Whilst promoting the electron mobility classically would seem to be a detriment to HET systems, due to the reduction in current utilisation efficiency, it could also be a pathway to reducing the anode voltage of such a system, enabling the possibility of a direct drive architecture.

5. Conclusion

Unsteady forcing of the axial electric field was successfully demonstrated as a method for manipulating plasma turbulence within the azimuthal electric field of a cross-field E×B device in simulation using a reduced order 1D-3V electrostatic PIC model. Wider characterisation of the effects of unsteady forcing on the baseline test case for frequencies between 1×10^6 Hz and 1×10^{10} Hz at three different forcing amplitudes, $10\,\mathrm{V\,cm^{-1}}$, $50\,\mathrm{V\,cm^{-1}}$ and $100\,\mathrm{V\,cm^{-1}}$ led to a conclusion that a link between the electron cyclotron frequency Ω_{ce} and the frequency of maximum growthrate of the EDI $[\omega_R]_{max}$ exists, indicated by a reduction of the temporal spectral amplitude corresponding to $[\omega_R]_{max}$ for the EDI when forcing at the electron cyclotron frequency Ω_{ce} and vice versa. Investigating the effects on azimuthal electric field spectral response to a forcing frequency three main frequency bands were identified: forcing within the range $\omega_{\mathrm{EF}} < \omega_{pi}$ led to a spectral amplitude reduction in the range ω_{pi} to ω_{E}. Forcing in the range of frequencies $\omega_{pi} < \omega_{\mathrm{EF}} < \omega_{\mathrm{E}}$ resulted in a peak in spectral amplitude at the forcing frequency and its harmonics and a spectral amplitude reduction in the range $\omega_{pi} < \omega_{\mathrm{EF}} < \omega_{\mathrm{E}}$. Damping of the

peak corresponding to the electron cyclotron frequency was observed as the forcing frequency approached ω_{E}. Forcing in the range $\omega_{\mathrm{E}} < \omega_{\mathrm{EF}}$ demonstrated frequency 'lock-in' behaviour which was observed for forcing frequencies close to electron cyclotron frequency. Forcing in this range also resulted in amplification of spectral amplitude of the peaks corresponding to the Hall circulation frequency and its resonances when forcing at said frequency.

The electron cross-field mobility was evaluated and compared to the baseline value for each forcing frequency. It was found that forcing at the frequency of the fundamental cyclotron harmonics $\omega_R(nk_0)$ resulted in a significant reduction in cross-field mobility. Two theories for the reduction were presented, one whereby forcing at these frequencies was thought to reduce the number of excited wavemodes in the plasma, preventing 'chaotic' superposition of different wavemodes that could cause unpredictable increases in amplitude of the electric field and corresponding cross-field mobility. The second theory supposed the reduction in cross-field mobility could result from forcing causing the electric field and the electron density distribution to oscillate out of phase with one another, reducing the resultant cross-field mobility. Conversely, forcing at frequencies close to the electron cyclotron frequency led to a significant increase in cross-field mobility, thought to be as a result of disruption to the circular motion of the electrons in the $\mathbf{E} \times \mathbf{B}$ field.

Future areas of interest diverging from these findings such as mapping of energy pathways between the axial electric field and azimuthal field could be researched further. Additional testing of these results on an expanded parameter set with an alternative baseline case would help to reinforce the conclusions made in this paper. Furthermore, testing these results on a higher order 2D model of the thruster which accurately models the non-uniform nature of the axial electric field could verify the results obtained for forcing at the frequencies of the fundemental cyclotron harmonics and electron cyclotron frequency. This would make way for experimental tests that may yield development of a high current utilisation efficiency HET or a direct drive HET system.

References

[1] Goebel D and Katz I 2008 *Fundamentals of Electric Propulsion: Ion and Hall Thrusters* (Jet Propulsion Laboratory)

[2] Morozov A and Savelyev V 2000 Fundamentals of Stationary Plasma Thruster Theory *Reviews of Plasma Physics* Reviews of Plasma Physics ed Kadomtsev B B and Shafranov V D (Boston, MA: Springer US) pp 203–391 ISBN 978-1-4615-4309-1 URL https://doi.org/10.1007/978-1-4615-4309-1_2

[3] Lev D, Myers R, Lemmer K, Kolbeck J, Koizumi H and Polzin K 2019 *Acta Astronautica* **159** 213–227 ISSN 00945765 URL https://linkinghub.elsevier.com/retrieve/pii/S0094576518319672

[4] Adamovich I, Agarwal S, Ahedo E, Alves L L, Baalrud S, Babaeva N, Bogaerts A, Bourdon A, Bruggeman P J, Canal C, Choi E H, Coulombe S, Donkó Z, Graves D B, Hamaguchi S, Hegemann D, Hori M, Kim H H, Kroesen G M W, Kushner M J, Laricchiuta A, Li X, Magin T E, Mededovic Thagard S, Miller V, Murphy A B, Oehrlein G S, Puac N, Sankaran R M, Samukawa S, Shiratani M, Šimek M, Tarasenko N, Terashima K, Thomas Jr E, Trieschmann J, Tsikata S, Turner M M, van der Walt I J, van de Sanden M C M and von Woedtke T 2022 *Journal of Physics D: Applied Physics* **55** 373001 ISSN 0022-3727, 1361-6463 URL https://iopscience.iop.org/article/10.1088/1361-6463/ac5e1c

[5] Hofer R 2004 *Development and Characterization of High-Efficiency, High-Specific Impulse Xenon Hall Thrusters* Ph.D. thesis University of Michigan

[6] Boeuf J and Garrigues L 2018 *Physics of Plasmas* **25** 061204 ISSN 1070-664X, 1089-7674 URL http://aip.scitation.org/doi/10.1063/1.5017033

[7] Boeuf J 2017 *Journal of Applied Physics* **121** 011101 ISSN 0021-8979, 1089-7550 URL http://aip.scitation.org/doi/10.1063/1.4972269

[8] Raitses Y, Kaganovich I, Khrabrov A, Sydorenko D, Fisch N and Smolyakov A 2011 *IEEE Transactions on Plasma Science* **39** 995–1006 ISSN 1939-9375 conference Name: IEEE Transactions on Plasma Science

[9] Sydorenko D, Smolyakov A, Kaganovich I and Raitses Y 2006 *Physics of Plasmas* **13** 014501 ISSN 1070-664X, 1089-7674 URL http://aip.scitation.org/doi/10.1063/1.2158698

[10] Sydorenko D, Smolyakov A and Kaganovich I 2008 *Phys. Plasmas* 8

[11] Taccogna F, Longo S, Capitelli M and Schneider R 2009 *Applied Physics Letters* **94** 251502 ISSN 0003-6951, 1077-3118 URL http://aip.scitation.org/doi/10.1063/1.3152270

[12] Lafleur T 2018 *Plasma Sources Sci. Technol.* 19

[13] Lampe M 1972 *Physics of Fluids* **15** 2356 ISSN 00319171 URL https://aip.scitation.org/doi/10.1063/1.1693879

[14] Forslund D, Morse R and Nielson C 1970 *Physical Review Letters* **25** 1266–1270 ISSN 0031-9007 URL https://link.aps.org/doi/10.1103/PhysRevLett.25.1266

[15] Croes V, Lafleur T, Bonaventura Z, Bourdon A and Chabert P 2017 *Plasma Sources Science and Technology* **26** 034001 ISSN 1361-6595 URL https://iopscience.iop.org/article/10.1088/1361-6595/aa550f

[16] Tavant A, Croes V, Lucken R, Lafleur T, Bourdon A and Chabert P 2018 *Plasma Sources Science and Technology* **27** 124001 ISSN 1361-6595 URL https://iopscience.iop.org/article/10.1088/1361-6595/aaeccd

[17] Wu J, Lu X, Denny A, Fan M and Wu J 1998 *Journal of Fluid Mechanics* **371** 21–58 ISSN 0022-1120, 1469-7645 URL https://www.cambridge.org/core/product/identifier/S0022112098002055/type/journal_article

[18] Knoll A, Bradley J, Ridgers C, Eastwood J and Bowden M 2021 Taming turbulence in magnetized plasmas using unsteady electrostatic forcing

[19] Gary S and Sanderson J 1970 *Journal of Plasma Physics* **4** 739–751 ISSN 0022-3778, 1469-7807 URL https://www.cambridge.org/core/product/identifier/S0022377800005390/type/journal_article

[20] Ducrocq A, Adam J C, Héron A and Laval G 2006 *Physics of Plasmas* **13** 102111 ISSN 1070-664X, 1089-7674 URL http://aip.scitation.org/doi/10.1063/1.2359718

[21] Cavalier J, Lemoine N, Bonhomme G, Tsikata S, Honoré C and Grésillon D 2013 *Physics of Plasmas* **20** 082107 ISSN 1070-664X, 1089-7674 URL http://aip.scitation.org/doi/10.1063/1.4817743

[22] Janhunen S, Smolyakov A, Chapurin O, Sydorenko D, Kaganovich I and Raitses Y 2018 *Physics of Plasmas* **25** 011608 ISSN 1070-664X, 1089-7674 URL http://aip.scitation.org/doi/10.1063/1.5001206

[23] Lafleur T, Baalrud S and Chabert P 2017 *Plasma Sources Science and Technology* **26** 024008 ISSN 1361-6595 URL https://iopscience.iop.org/article/10.1088/1361-6595/aa56e2

[24] Lafleur T, Baalrud S D and Chabert P 2016 *Physics of Plasmas* **23** 053503 ISSN 1070-664X, 1089-7674 URL http://aip.scitation.org/doi/10.1063/1.4948496

[25] Bittencourt J 2004 *Fundamentals of Plasma Physics* (New York, NY: Springer New York) ISBN 978-1-4419-1930-4 978-1-4757-4030-1 URL http://link.springer.com/10.1007/978-1-4757-4030-1

[26] Boeuf J 2014 *Frontiers in Physics* **2** ISSN 2296-424X URL http://journal.frontiersin.org/article/10.3389/fphy.2014.00074/abstract

[27] Lafleur T, Baalrud S and Chabert P 2016 *Physics of Plasmas* **23** 053502 ISSN 1070-664X, 1089-7674 URL http://aip.scitation.org/doi/10.1063/1.4948495

[28] Bezanson J, Edelman A, Karpinski S and Shah V 2020 Julia Programming Language URL https://www.JuliaLang.org

[29] 2018 LANDMARK URL https://www.landmark-plasma.com

[30] Birdsall C and Langdon A 1985 *Plasma physics via computer simulation* (New York: McGraw-Hill) ISBN 978-0-07-005371-7

[31] Faraji F, Reza M and Knoll A 2022 *Journal of Applied Physics* **131** 193302 ISSN 0021-8979, 1089-7550 URL https://aip.scitation.org/doi/10.1063/5.0090853

[32] Bird G 1994 *Molecular gas dynamics and the direct simulation of gas flows* (*Oxford engineering science series* no 42) (Oxford : New York: Clarendon Press ; Oxford University Press) ISBN 978-0-19-856195-8

[33] Tejeda J, Reza M, Faraji F and Knoll A 2022 *Acta Astronautica* **194** 145–161 ISSN 00945765 URL https://linkinghub.elsevier.com/retrieve/pii/S009457652200042X

[34] Frigo M and Johnson S 1998 FFTW: an adaptive software architecture for the FFT *Proceedings of the 1998 IEEE International Conference on Acoustics, Speech and Signal Processing, ICASSP '98 (Cat. No.98CH36181)* vol 3 (Seattle, WA, USA: IEEE) pp 1381–1384 ISBN 978-0-7803-4428-0 URL http://ieeexplore.ieee.org/document/681704/